Published paper
Bigg, G.R., Clark, C.D. and Hughes, A.L.C. (2008) *A last glacial ice sheet on the Pacific Russian coast and catastrophic change arising from coupled ice–volcanic interaction.* Earth and Planetary Science Letters, 265 (3-4). pp. 559-570.

A last Glacial ice sheet on the Pacific Russian coast and catastrophic change arising from coupled ice-volcanic interaction

G.R. Bigg[a *], C.D. Clark[a] and A.L.C. Hughes[a]

[a]*Department of Geography, University of Sheffield, Winter Street, Sheffield S10 2TN, U.K.*

Corresponding author: e-mail address grant.bigg@sheffield.ac.uk (G.R. Bigg)

Published in Earth & Planetary Science Letters, 2008, **265**: 559-570, doi10.1016/j.epsl.2007.10.052

Abstract

Controversy exists over the extent of glaciation in Eastern Asia at the Last Glacial Maximum: complete ice sheet cover vs. restricted mountain icefields (an area discrepancy equivalent to 3.7 Greenland Ice Sheets). Current arguments favour the latter. However, significant last glacial ice-rafted debris (IRD) exists in NW Pacific ocean cores, which must have been sourced from a major ice sheet somewhere bordering the North Pacific. The origin of this IRD is addressed through a combination of marine core analysis, iceberg trajectory modelling and remote sensing of glacial geomorphology. We find compelling evidence for two stages of glaciation centred on the Kamchatka area of maritime southeast Russia during the last glacial, with ice extent intermediate in size between previous maximum and minimum reconstructions. Furthermore, a significant increase in iceberg flux precedes, and accompanies, a substantial marine core ash deposit at around 40ka BP. We speculate that rapid decay of the first stage of the ice sheet may have triggered substantial volcanic activity.

Keywords: Kamchatka, ice sheet, Last Glacial, volcanic ash, ice-rafted debris, ODP Site 883

1. Introduction

Polarised views of glaciation in NE Asia during the last glacial period exist in the literature. One proposes extensive glaciation in the region at the Last Glacial Maximum (LGM) in the Siberian and Pacific Arctic [1] and the Sea of Okhotsk area [2] (Fig. 1). The more popular counterview is for limited mountain-based glaciation in some areas of NE Asia, and no marine-based or Beringian ice cover [3-5]. Improved understanding of the extent of ice in this region is important for palaeoclimate models because a significant NE Asian Ice Sheet would affect the climate well beyond the physical limits of the ice itself [6]. Climate models suggest a tendency for ice sheet growth over NE Asia during the onset of the last glaciation [7]. Also, there is discrepancy between global syntheses of ice sheet volume and observed sea level [8], particularly during the growth phase of the last glaciation [9]. These factors motivate a re-examination of the history of glaciation during the Late Quaternary in this area.

There is increasing field evidence to support the restricted glaciation view: tundra-style vegetation conditions, for example, have been reconstructed in Beringia at the LGM [10]. Geomorphological mapping from satellite images and relative age dating has suggested that the Late Weichselian (locally Sartan) glaciation in Chukotka was less extensive than previous Pleistocene glaciations [11]. A mapping study of moraines in central Chukotka, coupled with cosmogenic dating, suggested that moraines there are older than middle Pleistocene in age [4] while a synthesis of observations of glaciations in Russian and Alaskan Beringia only found evidence for limited mountain-valley glaciation [12]. It is worth noting, however, that recent discoveries based on the bathymetry offshore of NW Alaska have suggested rather more glacial ice in this region than previously supposed [13].

Much of the evidence outlined above is from mountains north of the Anadyr River (65^{o}N; Fig. 1). South of the Anadyr there is, however, evidence for glaciers approaching the coast [14] and also evidence for Late Weichselian glaciation centred on the Chers Range north of the Sea of Okhotsk and coastal uplands south of the Anadyr River through the Koryak upland and Kamchatka [15]. Ice in the Koryak region is known to have reached the coast during the LGM [16] and there are a number of other possible places along the Pacific coast to southern Kamchatka where ice may have reached the coast [17]. Weichselian (Sartan) glaciation has also been identified in the mountains of southern Kamchatka, and tephra and palaeosol relationships with glacial deposits have been used to argue that glaciers nearly reached Kamchatka’s west coast but probably before 40kyr BP [18]. In addition, clastic sedimentation in the open ocean of the Northwest Pacific is dominated by ice rafting [19]. The literature describing IRD lithologies strongly affirms that through the Quaternary NW Pacific IRD originated from Kamchatka and eastern Siberia [19-22], while NE Pacific IRD came from Alaska [22-24], with no evidence of source mixing. This has also been found to be the case for the last glacial period [19, 22, 24], and evidence demonstrates that IRD magnitudes were similar to those found in the Atlantic [25]. The state of the volcanic rock particles in the IRD suggests that most of it has been reworked before marine deposition, rather than being freshly added [20].

In summary, there appears to be a dichotomy in the evidence for Weichselian (Sartan) glaciation over NE Asia: limited alpine-style glaciers versus major ice sheets reaching the ocean. We will examine this conundrum through a combination of marine and terrestrial investigations, beginning by examining the IRD record of the LGM North Pacific.

2. The observed distribution of Last Glacial IRD in the North Pacific

In the literature there are relatively few measurements of IRD at the LGM in the Pacific, and the units of measurement vary from counts of the number of lithic grains per gram, through to the percentage weight of IRD in the sediment, to concentrations of IRD expressed in g cm^{-2} kyr^{-1}. Even the latter sedimentation rate is not easily comparable from one site to another as different workers take different size ranges of material as their definition of IRD, varying from >62 μm to 250-2000 μm. However, sufficient cases of multiple forms of measurement exist that a judgement of the relative amounts of IRD in different locations can be made. This was strengthened, and extended, by comparison of the visual core log for every ODP and DSDP bore hole in the North Pacific. As a comparison of IRD magnitude, we used maps of the Northeast Atlantic IRD concentration for several time periods during the last two glaciations [26], with a uniform measure of IRD concentration in g cm^{-2} kyr^{-1} for the 63-2000 μm size fraction. In Fig. 2 we compare our assessment of the relative magnitudes of LGM IRD in the North Pacific with a similar assessment in the North Atlantic, combining the North Atlantic maps mentioned above with higher time resolution data from a number of papers. This was done because the early work, [26], is an average over the time period 25-13 ^{14}C kyr and so will be an over-estimate of the LGM flux because of the contamination of IRD peaks from the two Heinrich events H_1 and H_2. For our purposes the LGM covers a period of ~2kyr centred on 21ka BP. The data that has contributed to Fig. 2 is listed in the Supplementary Material, Table S1, with a description of how the various types of measurements were calibrated for the purposes of the broad categories used in Fig. 2.

While the North Atlantic had much more extensive regions of high IRD flux at the LGM than the Pacific, there is a broad similarity in the extent of IRD between the ocean basins. The peaks are similar in magnitude: at core RAMA 44PC near 53°N, 164.6°E there were at times 10 g cm^{-2} kyr^{-1} in the size fraction > 150 µm [27], even around 15 kyr BP, very similar to the highest LGM IRD levels of the central Atlantic [26, 28]. Some values in the western Pacific are comparable to those in the NE Atlantic, while IRD levels in the northern Gulf of Alaska approach those in the central Atlantic (compare [21] with [26]).

The LGM IRD distribution in the Pacific is thus consistent with a major flux of icebergs from North America and significant, if smaller, fluxes from the coast of the Kamchatka Peninsula and northwards. Combined with the already cited provenance evidence this suggests significant LGM ice flux to the sea from these parts of NE Russia. In the next section we will use an iceberg trajectory model to test these hypotheses about the origin of icebergs in the LGM North Pacific.

3. Modelling the distribution of Last Glacial IRD in the North Pacific

We can examine where we would expect to find IRD in the glacial North Pacific through seeding the ocean's perimeter with icebergs and using an iceberg trajectory model [29], forced by simulated glacial ocean currents, to predict the probable distribution of icebergs. The iceberg trajectory model allows a suite of icebergs of different sizes to move, and melt, according to the dynamics and thermodynamics of the ocean, atmospheric and sea-ice forcing. Ten size classes of icebergs were released, varying from approximately 100 m to 1500 m in length; ignoring giant icebergs does not seriously bias the equatorward limits produced by the model [30]. The icebergs may overturn and be grounded until melted sufficiently for refloating. The sites for release were generally chosen to cover all feasible areas in a uniform manner, although the NE Pacific icebergs were preferentially seeded at locations likely to be major source areas [31].

The glacial global ocean circulation could at different times in the last glacial period be in one of three states: an intermediate North Atlantic sinking state forming moderate amounts of North Atlantic intermediate water; a fresh North Atlantic with deep water formation only in the Southern Hemisphere; and a less likely state with enhanced North Atlantic sinking. Each of these modelled LGM states [32-33] has similar circulation in the North Pacific. This can be inferred from Fig. 3 where we plot iceberg trajectories across the glacial North Pacific for each glacial ocean state. A range of palaeoclimate models give similar atmospheric forcing predictions for the LGM over the North Pacific, and particularly did not place the Aleutian Low noticeably further south [34], to those used to force our ocean states. We therefore believe that our conclusions are robust and independent of the real glacial ocean circulation.

Each of the ocean states shows a similar pattern of iceberg drift. Icebergs from the Gulf of Alaska are predominantly trapped in a cyclonic coastal current and only penetrate the interior of the eastern Pacific from along the Aleutian arc. No icebergs deriving from the North American ice sheets, including the Aleutian arc, penetrate into the western Pacific under any ocean circulation scenario.

While the simulations in Fig. 3 assume an average LGM climate, and so the real distribution of IRD will be more dispersed, they offer clear markers for comparison with glacial IRD observations. In the eastern Pacific, Fig. 3 suggests that LGM icebergs originating from North America would have been kept close to the coast and could not leave the coastal current until it swept southwest along the Aleutians. This region has few IRD measurements, but what data there is in Fig. 2 in the NE Pacific is consistent with this reconstruction. In the western Pacific Fig. 3 suggests that icebergs from the Pacific coast of Kamchatka would have also been kept close to the coast before entering a narrow southward current. Again, this is consistent with Fig. 2, but the key region is poorly sampled and the main export route south may have been missed by the existing set of observations. Both modelling and core lithological data therefore supports the separation of sources of LGM IRD between east and west Pacific, with IRD in the west originating from the Pacific coastline of Siberia from the Anadyr River to Kamchatka. We take this as a strong argument for a large ice mass delivering icebergs to the Russian Pacific; we now examine the terrestrial evidence.

4. Glacial geomorphological evidence for ice masses in the vicinity of Kamchatka

A useful overview of LGM and Quaternary maximum ice extents, insofar as this is known, has been recently compiled [35]. For Kamchatka, an LGM icefield centred on, and mostly restricted to, the mountains of the main median ridge and outliers is reconstructed, with ice reaching the coast as outlet glaciers in just a few places (Fig. 1). This was also taken to be the maximum Quaternary ice extent, in contradiction to the existing work of others ([15], [18]).

We utilised around 50 Landsat ETM+ satellite images (resolution of 15 – 30 m), digital elevation models (DEM) derived from the Space Shuttle Topographic Mission (SRTM) at around 90 m resolution, and bathymetric data of around 2.5 km resolution (from GEBCO) to systematically search for glacial geomorphological evidence using the techniques of Clark

[36], to test and constrain palaeo-ice extents. Here we focus on moraines, as these are a primary indicator of recent palaeo-ice extent. Figures S1 and S2 in the on-line supplementary information show large end and lateral moraines (kms wide, tens of kms long), found in most major valleys of the main median divide of Kamchatka. These are consistent with a recent reconstruction [35]. However, we have also found moraines and lateral meltwater channels (Figs. S3-S5) that indicate a more extensive ice mass, summarised in Fig. 4, in which ice reached the Kamchatkan coastline, on both the east (Figs. S3-S4) and west (Fig. S5) sides of the peninsula, in many places. Moraines mapped in Fig. 4 thus provide unequivocal evidence that Kamchatkan ice, at some time, was not just restricted to the main mountain divide but got at least as far as the coast in many places on both the Pacific and Sea of Okhotsk coastlines, supporting and considerably extending previous fieldwork [18].

Of the 105 moraines identified (Fig. 4) we note that their spatial and elevation distribution indicate two systematic contexts: one group immediately adjacent to the major mountain belts and at elevations of around 300 m above sea level, and another group some 60-80 km distant, close to the coast, at elevations of around 50 m. As moraines record stillstands of ice margins, we infer that two snapshots of glaciation are recorded by the two moraine systems. A major ice field existed along the length of the Kamchatkan Mountains, and was stabilised in this position for a time long enough to build the substantial moraine systems mapped. At some time prior to this a much more extensive ice sheet existed, also centred on the Kamchatkan Mountains but reaching the coastline. The poor resolution of the available bathymetric data does not help to reveal its maximum extent. A reasonable presumption, however, is that ice extended beyond the shoreline terminating as an iceberg-calving front. In places, lateral meltwater channels and moraines indicate ice extended offshore (Figs. S3 and S4). Once the margin backstepped onto land we infer it stabilised, producing the coastal system of end moraines (Fig. 4).

From previous work and our glacial geomorphological evidence we reconstruct two stages of glaciation (Fig. 1). The evidence requires an earlier, and larger, ice sheet whose margin extended at least to the coastline around the coasts of Kamchatka and Koryak producing an extensive marine-terminating ice margin. This stage was likely to include ice streams, and therefore high potential for iceberg delivery to the ocean. A later, more restricted glaciation also occurred, with montane ice fields and some marine-terminating outlets in NE Kamchatka and along the Koryak coastline. The mountain icefield complex of Kamchatka-Koryak is estimated to have covered 0.27 million km^2, while the full Kamchatka-Koryak Ice Sheet covered 0.63 million km^2, about one third the size of today's Greenland Ice Sheet.

Geochronometric dates to fix the moraines in time are lacking, but we would expect well-preserved moraines to date from the last glaciation [11]. To our knowledge there is only one study [18] that provides the only published dating. This paper concluded that two moraines and terraces whose positions are broadly consistent with the montane-icefield glaciation are of ‘Late Pleistocene’ age. Another moraine, one which we have also mapped, on the west coast (~ 156° 15’E, 52° 51’N) was placed as being older than 40 ka BP on the basis of an overlying tephra of this age. In the absence of a good time control on changing ice extent from the terrestrial record we turn next to the better chronological control found in the marine record.

5. Variation in Pacific IRD during the last glacial cycle

Most sites across the Pacific show evidence for peaks in IRD during the last glacial cycle, particularly around 40 kyr BP, which are some 2-4 times above the levels seen around 18kyr BP [21, 24-25, 37-38]. ODP core 883D (51°N, 168°E) has proven a major focus for a number of these Quaternary palaeoclimate studies in the NW Pacific. We took samples of 10 cm^3 every 2 cm in its top 2.74 m, reaching back to ~ 43 kyr BP so as to include the time period of highest and most persistent IRD during the second half of the last glacial cycle [38]. We revised the core’s age model by recalibrating the 19 radiocarbon dates available for this section of core [38] using the calibration programme OxCal [39], a reservoir age of 830±270yr (the mean of suggested reservoir ages for North Pacific sites [40]), and the Lake Suigetsu extension of the INTCAL98 calibration curve [41]. This provides temporal sample intervals of 300-1000 years. We counted the number of clastic grains and ash grains in the >150µm fraction of each sample, and expressed this as a function of dry bulk mass of the whole sample. Ash this size is likely to be ice-rafted this far from Kamchatka [42], particularly in bulk, but we cannot rule out the possibility of an airfall origin in such an area of explosive volcanism. It is therefore reasonable to separate out the ash from the clastic material.

In Fig. 5 we show the number of both lithic and ash grains per unit dry weight of sediment. At the LGM there are ~200 (non-ash) lithic grains per gram of sediment, a number representative of the background level throughout the period shown and comparable to LGM values found in other areas of the NW Pacific [43], and to LGM values in the eastern central North Atlantic [28].

However, as well as minor fluctuations, there are some major increases in IRD flux, at ~ 25 kyr, 32.5 kyr, 37.5 kyr and 39.3 kyr BP (‘H’ in Fig. 5). Note also that the major ash event in the record coincides with our earliest, and largest, IRD event, suggesting possible ice-volcanic interaction. However, the onset of this peak ('O' in Fig. 5) shows a strong increase in IRD well before significant ash input (which started around 39.7 kyr BP), suggesting that a major ice collapse over the Kamchatka-Koryak region pre-dates any volcanic eruption sequence. The magnitude of the 39.3 kyr BP IRD peak is similar to levels reached in the eastern Atlantic during H_1 and H_2 [28] and in the Faroe-Shetland Channel during major iceberg discharge events [44].

To put this spike in IRD and ash into context within the longer record at site 883D we show coarser measurements [38] back to ~ 62 kyr BP (Fig. 6). It is also instructive to examine the Gamma Ray Attentuation Porosity Evaluator (GRAPE) bulk density record for this, and other, cores at this location [25], as GRAPE density is proportional to core terrigenous material [25]. These measurements go to 10 m depth (~ 200 kyr BP), These records show the unusual nature of the peak around 40kyr BP, although there appear to be occasional similar events in the previous glacial cycle [25] and lesser, but still large, anomalies earlier in the Weichselian (Sartan; Fig. 6). Thus, the temporal variation of IRD at ODP site 883, combined with the modelled iceberg trajectories, indicates that the maximum Weichselian (Sartan) ice flux from the Kamchatka-Koryak region occurred early in the glacial cycle, with a major and sustained period of collapse over ~41-36 kyr BP, initiated by a massive iceberg discharge event. Two further, much less extreme, events followed before a final retreat of glaciers from the NW Pacific shoreline at ~ 14 kyr BP.

6. Conclusion

The marine record of the North Pacific incontrovertibly demonstrates that there were major IRD fluxes issuing into the glacial ocean from surrounding landmasses. All previous lithological analyses [19-22, 24], a previous major discussion of Weichselian (Sartan) IRD in the NW Pacific [25] and our iceberg trajectory modelling strongly support a Northeast Asian origin for IRD found in the NW Pacific. Persuasive chronological control in NW Pacific ODP Core 883D allows confidence in the existence of a major iceberg discharge phase around 40 kyr BP, comparable in magnitude to that of Heinrich events in the Atlantic, followed by much smaller events until the end of a marine-terminating ice presence ~ 14 kyr BP. On land, the one reliable date to tie the two stage Kamchatkan glacial geomorphological evidence within the Quaternary shows that the montane glaciation stage in South Kamchatka dates after 40 kyr BP while the western, coastal phase pre-dates this [18]. Palaeoclimate data for the region is sparse prior to 20 kyr BP but pollen records north of the Sea of Okhotsk suggest a cold phase during 45-39 kyr BP, followed by warmer and moister conditions until 32 kyr BP [45]. All these lines of evidence lead us to present the hypothesis that a large Kamchatka-Koryak Ice Sheet (KKIS) existed during the Weichselian, attaining its maximum configuration sometime prior to 40 kyr BP, rather than at the LGM. Both the marine and terrestrial data are consistent with such an Ice Sheet experiencing a major purging around this time. We further hypothesise that subsequently, and after much ice margin retreat, montane-based icefields stabilised over parts of the area, and this, reduced, stage is presumed to be representative of the (global) LGM at 18 kyr BP.

The early stage, KKIS, glaciation is estimated to cover in excess of 0.6 million km^2, with extensive marine-terminating ice margins. Montane-based icefields (covering an estimated 0.27 million km^2) characterise the later stage, with some ice outlets still reaching the sea. We therefore find elements of truth in both extremes of the Pacific Russian ice sheet controversy [1, 4]. While there is little evidence for extensive ice further north over Beringia and NE Russia [3, 5] our marine and terrestrial evidence demonstrates a significant ice sheet over parts of maritime Pacific Russia south of the Anadyr River. However, we have shown that this ice was less extensive at the LGM than earlier in the Last Glacial. The Weichselian (Sartan) glacial state of the region west of the reconstructed landward margin in Fig. 1 remains unresolved, as here there is contradictory evidence in the local geomorphology and palaeobiology suggesting the possible presence of significant ice masses, but not complete cover (for example contrast [15], and on-line Fig. S6, with [10]). Our reconstruction nevertheless points towards a resolution of a long-standing controversy, and in reconciling the marine and terrestrial evidence of Weichselian (Sartan) ice sheet activity. These findings also contribute to reconciling global ice volumes with changes in sea level during the Last Glacial. On the latter issue there was an approximately 25 m rise in sea level during 40-39 kyr BP [46], at least 5% of which could be explained by the change in the Kamchatka-Koryak Ice Sheet. Given our conclusion that a large ice sheet covered Kamchatka and Koryak, we speculate that more substantial ice masses may also have existed over parts of the mountains to the north of the Sea of Okhotsk (see question marks in Fig. 1), and that additional contributions to sea level rise at this time may be attributed to its melting. There is considerable scope for future fieldwork in eastern Russia to resolve the dating and ice extent issues of the wider area and to test and constrain our hypothesised KKIS reconstruction.

The correspondence of the largest ice discharge and ash events in core ODP 883D (Fig. 5), yet the former's onset some centuries before the ash event is intriguing. We speculate that there may have been a feedback mechanism between ice sheet loading and volcanic activity leading to this relationship. The purging event with greatly enhanced iceberg discharge into the Pacific must have greatly reduced the volume of the KKIS. Its cause may have been a consequence of enhanced geothermal heating of basal ice producing wholesale ice streaming or ice sheet binge-purge oscillations [47]. Whatever the origin, we hypothesise that reduction of the ice load over southern Kamchatka for 500-1000 years may have promoted volcanic activity, as has been seen in other contexts in Iceland [48] and eastern California [49]. Terrestrial evidence shows that there was volcanic activity around 40kyr BP greater than anything subsequently experienced for southern and eastern Kamchatka and the northern Kurile Islands, with multiple examples of caldera formation occurring over a narrow time frame around and just after 40 kyr BP [50]. While at least some of these appear not to have been associated with magmatic activity directly [51], we note that there was a coincident peak in volcanic sulphate deposits in the Greenland GISP2 ice core [52]. It is also supportive to our hypothesis that a number of previous major IRD peaks in the NW Pacific during the past two glacial cycles have been accompanied by significant ash deposits (Fig. 6; [25]). However, the exact origin of ash in the sedimentary record of the region varies significantly with space and time and must arise from a set of local eruptions, and dispersal mechanisms, rather than one gigantic eruption covering the whole area in uniform ash. Thus the geochemical signatures, shown in Table 1, of the mid-Weichselian (Sartan) K2 and K3 ash spikes in the Sea of Okhotsk [53], the southwestern Kamchatkan pre-40kyr BP tephra [18] and the 40 kyr BP spike at ODP Site 883 [54] are all distinct,

Although further work is needed to confirm this ice-volcanism speculation, we suggest that volcanic activity could have been triggered by, and have prolonged, the Ice Sheet collapse at ~ 40 kyr BP, leading to a new, much reduced, ice mass. The more minor waxing and waning of the ice sheet suggested by the smaller IRD peaks post-35 kyr BP (Fig. 5) is not associated with ash deposit fluctuation and so also awaits further investigation.

Acknowledgements

This research used samples provided by the Ocean Drilling Program (ODP). ODP is sponsored by the U.S. National Science Foundation (NSF) and participating countries under management of Joint Oceanographic Institutions (JOI), Inc. ALCH gratefully acknowledges the Natural Environmental Research Council who part-funded an MSc in Quaternary Science at Royal Holloway, University of London, where part of this work was undertaken. We would like to thank Mark Maslin, who acted as internal supervisor for ALCH during her MSc, and Paul Coles and Graham Allsopp and Paul Coles, who prepared the diagrams. We would also like to thank Thorsten Kiefer who provided the radiocarbon dates on which the age model for Core 883 was based and the data from which Fig. 6 was produced.

References

[1] M.G. Grosswald, T.J. Hughes, The Russian component of an Arctic Ice Sheet during the Last Glacial Maximum, Quater. Sci. Rev. 21 (2002) 121-146.

[2] M.G. Grosswald, T.J. Hughes. “Back-arc” marine ice sheet in the Sea of Okhotsk. Russ. J. Earth Sci. 7 (2005) doi:10.2205/2005ES000180.

[3] J. Brigham-Grette, D.M. Hopkins, V.F. Ivanov, A. Basilyan, S.L. Benson, P. Heiser, V. Pushkar, Last interglacial and sea level history of coastal Chutotka Peninsula and St. Lawrence Island, western Beringia, Quater. Sci. Rev. 20 (2001) 419-436.

[4] J. Brigham-Grette, L.M. Gualtieri, O.Yu. Glushkova, T.D. Hamilton, D. Mostoller, A. Kotov, Chlorine-36 and ^{14}C chronology support a limited last glacial maximum across central Chutotka, north-eastern Siberia, and no Beringian ice sheet, Quater. Res. 59 (2003) 386-398.

[5] L. Gualtieri, S. Vartanyan, J. Brigham-Grette, M. Patricia, P.M. Anderson, Pleistocene raised marine deposits on Wrangel Island, NE Siberia: implications for Arctic ice sheet history, Quater. Res. 59 (2003) 399-410.

[6] B. Felzer, Climate impacts of an ice sheet in East Siberia during the Last Glacial Maximum, Quater. Sci. Rev. 20 (2001) 437-447.

[7] Z. Wang, A.-S.B. Cochelin, L.A. Mysak, Y. Wang, Simulation of the last glacial inception with the green McGill Paleoclimate Model, Geophys. Res. Lett. 32 (2005) doi:10.1029/2005GL023047.

[8] C. Zweck, P. Huybrechts, Modelling of the northern hemisphere ice sheets during the last glacial cycle and glaciological sensitivity, J. Geophys. Res. 110 (2005) doi:10.1029/2005D07103.

[9] S.J. Marshall, Modelled nucleation centres of the Pleistocene ice sheets from an ice sheet model with subgrid topographic and glaciologic parameterizations, Quater. Int. 95/6 (2002) 125-137.

[10] L.B. Brubaker, P.M. Anderson, M.E. Edwards, A.V. Lozhkin, Beringia as a glacial refugium for boreal trees and shrubs: new perspectives from mapped pollen data, J. Biogeogr. 532 (2005) 833-848.

[11] P.M. Heiser, J.J. Roush, Pleistocene glaciations in Chutotka, Russia: moraine mapping using satellite synthetic aperture radar (SAR) imagery, Quater. Sci. Rev. 20 (2001) 393-404.

[12] O.Yu. Glushkova, Geomorphological correlation of Late Pleistocene glacial complexes of Western and Eastern Beringia, Quater. Sci. Rev. 20 (2001) 405-417.

[13] J.C. Hill, N.W. Driscoll, J. Brigham-Grette, J.P. Donnelly, P.T. Gayes, L.D. Keigwin. New evidence for high discharge to the Chukchi Shelf since the Last Glacial Maximum. Quater. Res., in press (2007) doi:10.1016/j.yqres.2007.04.004.

[14] A.V. Alfimov, D.I. Berman, Beringian climate during the late Pleistocene and Holocene, Quater. Sci. Rev. 20 (2001) 127-134.

[15] S.A. Arkhipov, L.I. Isayeva, V.G. Bespaly, O. Glushkova, Glaciation of Siberia and north-east USSR, Quater. Sci. Rev. 5 (1986) 463-474.

[16] L. Gualtieri, O. Glushkova, O., J. Brigham-Grette. Evidence for restricted ice extent during the last glacial maximum in the Koryak Mountains of Chukotka, far eastern Russia. Geol. Soc. Amer. Bull. 112 (2000) 1106– 1118.

[17] D.H. Mann, T.D. Hamilton. Late Pleistocene and Holocene paleoenvironments of the North Pacific coast. Quarter. Sci. Rev. 14 (1995) 449– 471.

[18] R. Bäumler, W. Zech, Quaternary paleosols, tephra deposits and landscape history in South Kamchatka, Russia, Catena 41 (2000) 199-215.

[19] V.P. Nechaev, A.V. Sorochinskaya, I.B. Tsoy, S.A. Gorbarenko, Clastic components in Quaternary sediments of the northwest Pacific and their paleoceanic significance, Mar. Geol. 118 (1994) 119-137.

[20] J.R. Conolly, M. Ewing, Ice-rafted detritus in Northwest Pacific deep-sea sediments, in: J.D. Hays (Ed.), Geological Investigations of the North Pacific, Geological Society of America Memoir 126 (1970) pp. 219-231.

[21] K.E. St. John, L.A. Krissek, Regional patterns of Pleistocene ice-rafted debris flux in the North Pacific, Paleoceanogr. 14 (1999) 653-662.

[22] B.C. McKelvey, W. Chen, R.J. Arculus, Provenance of Pliocene-Pleistocene ice-rafted debris, Leg 145, Northern Pacific, in: D.K. Rea, I.A. Basov, D.W. Scholl, J.F. Allan (Eds.), Proceedings of the Ocean Drilling Program, Scientific Results, Leg 145, Texas College Station (1995) pp. 195-204.

[23] R. von Heune, J. Crouch, E. Larson, Glacial advance in the Gulf of Alaska area implied by ice-rafted material, Geological Society of America Memoir 145 (1976) pp. 411-422.

[24] A.T. Hewitt, D. McDonald, B.D. Bornhold, Ice-rafted debris in the North Pacific and correlation to North Atlantic climatic events, Geophys. Res. Lett. 24 (1997) 3261-3264.

[25] A.T. Kotilainen, N.J. Shackleton, Rapid climate variability in the North Pacific Ocean during the past 95,000 years, Nature 377 (1995) 323-326.

[26] W.F. Ruddiman, Late Quaternary deposition of ice-rafted sand in the sub-polar North Atlantic (lat 40^{o} to 65^{o}N), Geol. Soc. Amer. Bull. 88 (1977) 1813-1827.

[27] L.D. Keigwin, G.A. Jones, P.N. Floerich, A 15,000 year paleoenvironmental record from Meiji Seamount, far northwestern Pacific, Earth Planet. Sci. Lett. 111 (1992) 425-440.

[28] G. Auffret, S. Zaragosi, B. Dennielou, E. Cortijo, D. van Rooij, F. Grousset, C. Pujol, F. Eynaud, M. Siegert, Terrigeneous fluxes at the Celtic margin during the last glacial cycle, Mar. Geol. 188 (2002) 79-108.

[29] G.R. Bigg, M.R. Wadley, D.P. Stevens, J.A. Johnson, Modelling the dynamics and thermodynamics of icebergs, Cold Reg. Sci. Technol. 26 (1997) 113-135.

[30] R. Gladstone, G.R. Bigg, K.W. Nicholls, Icebergs and fresh water fluxes in the Southern Ocean, J. Geophys. Res. 106 (2001) 19903-19915.

[31] G.R. Bigg, M.R. Wadley, The origin and flux of icebergs released into the Last Glacial Maximum Northern Hemisphere oceans: the impact of ice-sheet topography, J. Quater. Sci. 16 (2001) 563-573.

[32] G.R. Bigg, M.R. Wadley, D.P. Stevens, J.A. Johnson, Simulations of two last glacial maximum ocean states, Paleoceanogr. 13 (1998) 340-351.

[33] M.R. Wadley, G.R. Bigg, E.J. Rohling, A.J. Payne, On modelling present day and last glacial maximum oceanic $\delta^{18}O$ distributions, Glob. Planet. Change 32 (2002) 89-109.

[34] M. Kageyama, P.J. Valdes, G. Ramstein, C. Hewitt, U. Wyputta. Northern hemisphere storm tracks in present day and last glacial maximum climate simulations: A comparison of the European PMIP models. J Clim. 12 (1999) 742-760.

[35] V. Zamoruyev, Quaternary glaciation of north-east Asia, in: J. Ehlers, P.L. Gibbard, (Eds.), Quaternary Glaciations – extent and chronology, Part III, Amsterdam, Netherlands, Elsevier (2004) pp. 321-323.

[36] C.D. Clark, Reconstructing the evolutionary dynamics of former ice sheets using multi-temporal evidence, remote sensing and GIS, Quater. Sci. Rev. 16 (1997) 1067-1092.

[37] D. Kent, N.D. Opdyke, M. Ewing, Climate change in the North Pacific using ice-rafted detritus as a climatic indicator, Geol. Soc. Amer. Bull. 82 (1971) 2741-2754.

[38] T. Kiefer, M. Sarnthein, h. Erlenkeuser, P.M. Grootes, A.P. Roberts, North Pacific response to millennial-scale changes in ocean circulation over the last 60 kyr, Paleoceanogr. 16 (2001) 179-189.

[39] C. Bronk Ramsey, OxCal radiocarbon calibration and stratigraphic analysis program, version 3.9, Research Laboratory for Archaeology, Oxford University, Oxford (2003) (www.rlaha.ac.uk).

[40] A.L.C. Hughes. The ice-rafted debris record of ODP Site 883, Northwest Pacific. MSc. Dissertation, Royal Holloway College, University of London (2004) 59 pp.

[41] H. Kitigawa, J. van der Plicht, Atmospheric radiocarbon calibration beyond 11,900 cal BP from Lake Suigetsu laminated sediments, Radiocarbon 42 (2000) 369-380.

[42] M.G. Wiesner, A. Wetzel, S.G. Catane, E.L. Listanco, H.T. Mirabueno. Grain size, areal thickness distribution and controls on sedimentation of the 1991 Mount Pinatubo tephra layer in the South China Sea. Bull. Volcanol. 66 (2004) 226-242.

[43] S.A. Gorbarenko, Stable isotope and lithological evidence of late-glacial and Holocene oceanography of the Northwest Pacific and its marginal seas, Quater. Res. 46 (1996) 230-250.

[44] S. Lassen, E. Jansen, K.L. Knudsen, A. Kuijpers, M. Kristensen, K. Christensen, Northeast Atlantic sea surface circulation during the past 30-10 ^{14}C kyr B.P., Paleoceanogr. 14 (1999) 616-625.

[45] P.M. Anderson, A.V. Lozhkin. The Stage 3 interstadial complex (Karginskii/middle Wisconsinan interval) of Beringia: variations in paleoenvironments and implications for paleoclimatic interpretations. Quater. Sci. Rev. 20 (2001) 93-125.

[46] E.J. Rohling, R. Marsh, N.C. Wells, M. Siddall, N.R. Edwards, Similar meltwater contributions to glacial sea level changes from Antarctic and northern ice sheets, Nature 430 (2004) 1016-1021.

[47] D.R. MacAyeal, Binge/purge oscillations of the Laurentide Ice Sheet as a cause of the North Atlantic's Heinrich events, Paleoceanogr. 8 (1993) 775-784.

[48] J. Maclennan, M. Jull, D. McKenzie, L. Slater, K. Gronvold, The link between volcanism and deglaciation in Iceland, Geochem. Geophys. Geosys. 3 (2002) doi:10.129/2001GC000282.

[49] A.M. Jellinek, M. Manga, M.O. Saar, Did melting glaciers cause volcanic eruptions in eastern California? Probing the mechanics of dike formation, J. Geophys. Res. 109 (2004) doi:10.1029/2004JB002978.

[50] O.A. Braitseva, I.V. Melekestsev, V.V. Ponomareva, L.D. Sulerzhitsky, Ages of calderas, large explosive craters and active volcanoes in the Kuril-Kamchatka region, Russia, Bull. Volcanol. 57 (1995) 383-402.

[51] V.V. Ponomareva, I.V. Melekestev, O.V. Dirksen. Sector collapses and large landslides on Late Pleistocene-Holocene volcanoes in Kamchatka, Russia. J Volcanol. Geotherm. Res. 158 (2006) 117-138.

[52] G.A. Zielinski, P.A. Mayewski, L.D. Meeker, S. Whitlow, M.S. Twickler, A 110,000-yr record of explosive volcanism, from the GISP2 (Greenland) Ice Core, Quater. Res. 45 (1996) 109-118.

[53] S.A. Gorbarenko, D. Nürnberg, A.N. Derkachev, A.S. Astrakhov, J.R. Southon, A. Kaiser. Magnetostratigraphy and tephrochronology of the Upper Quaternary sediments in the Okhotsk Sea: implication of terrigenous, volcanogenic and biogenic matter supply. Mar. Geol. 183 (2002) 107-129.

[54] L.-Q. Cao, R.J. Arculus, B.C. McKelvey. Geochemistry and petrology of volcanic ashes recovered from sites 881 through 884: a temporal record of Kamchatka and Kurile volcanism in: D.K. Rea, I.A. Basov, D.W. Scholl, J.F. Allan (Eds.), Proceedings of the Ocean Drilling Program, Scientific Results, Leg 145, Texas College Station (1995) pp. 345-381.

Figures

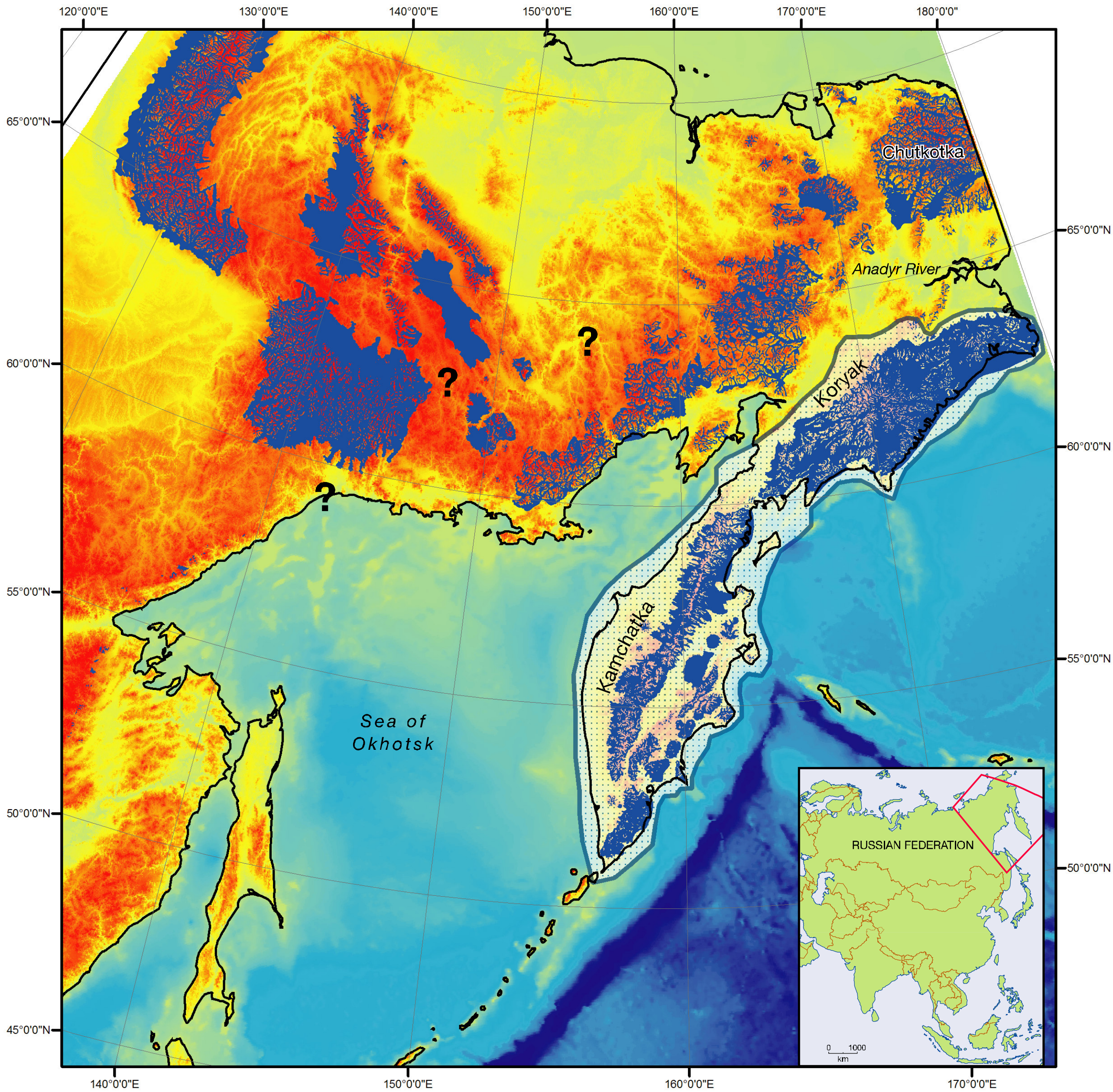

Fig. 1 Elevation rendition of NE Asia, showing main areas mentioned in the text. The Grosswald-reconstruction is not shown but places an extensive LGM ice sheet covering the entire mainland landmass, northern Arctic Shelf and the Sea of Okhotsk. The minimum view argues strongly against this and reconstructs restricted icefield complexes on the mountains, represented here by the synthesis of [35], marked in dark blue. The two stage model of glaciation reported in this paper is schematically shown by our maximal Kamchatka-Koryak Ice Sheet (stippled within a thick line), and the minimal reconstruction shown in dark blue. The question marks explain that we have not fully investigated north of the Sea of Okhotsk.

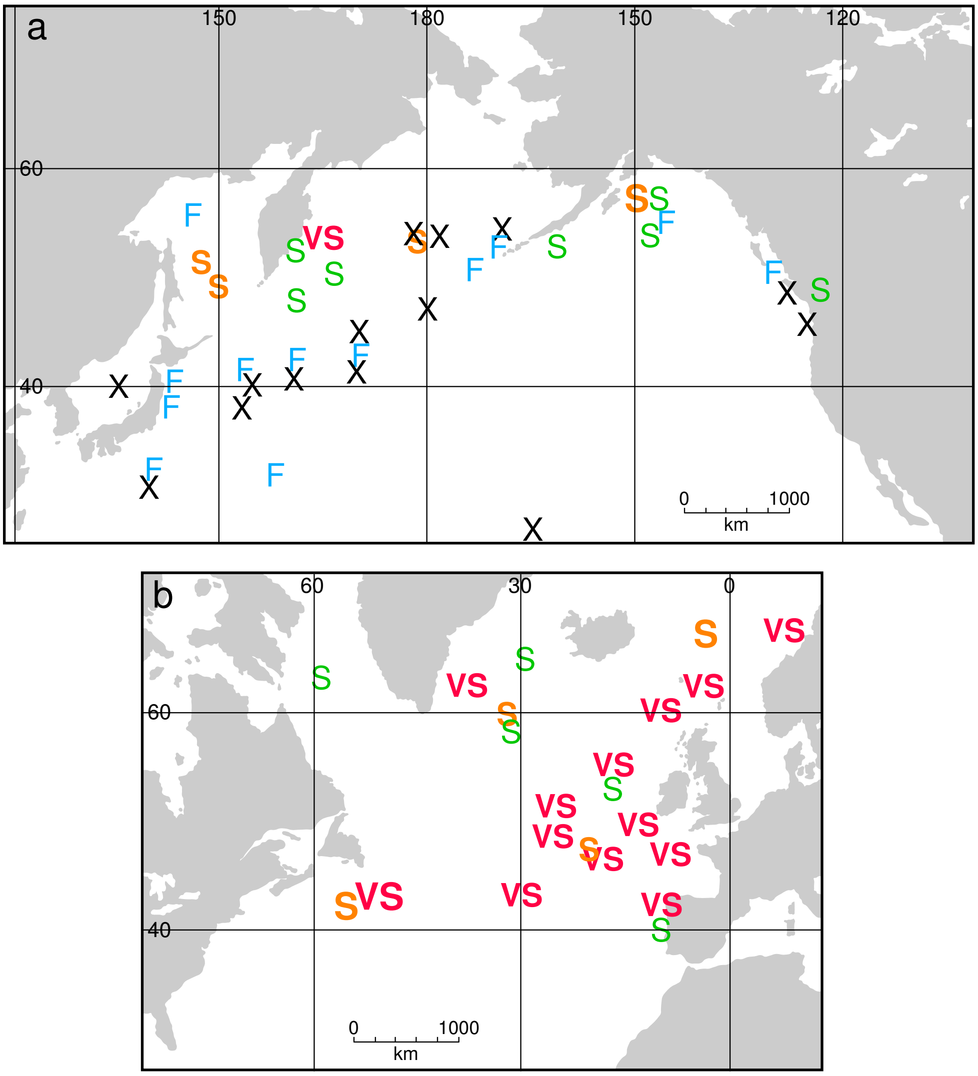

Fig. 2 Maps of extent and relative abundance of LGM IRD in the a) Pacific and b) North Atlantic. ‘X’ indicates no evidence of IRD, ‘F’ denotes concentrations < 50 $mgcm^{-2}kyr^{-1}$, ‘S’ ~ 50-250 $mgcm^{-2}kyr^{-1}$, ‘**S**’ ~ 250-1000 $mgcm^{-2}kyr^{-1}$ and ‘**VS**’ > 1000 $mgcm^{-2}kyr^{-1}$. It is clear that the extent and maximum concentrations of Pacific LGM IRD are similar to those of the North Atlantic. The data from which the maps were constructed is available as Supplementary Material in Table S1. The S at 51.2°N, 167.8°E shows ODP Site 883, a core from which is sampled in detail in Fig. 5.

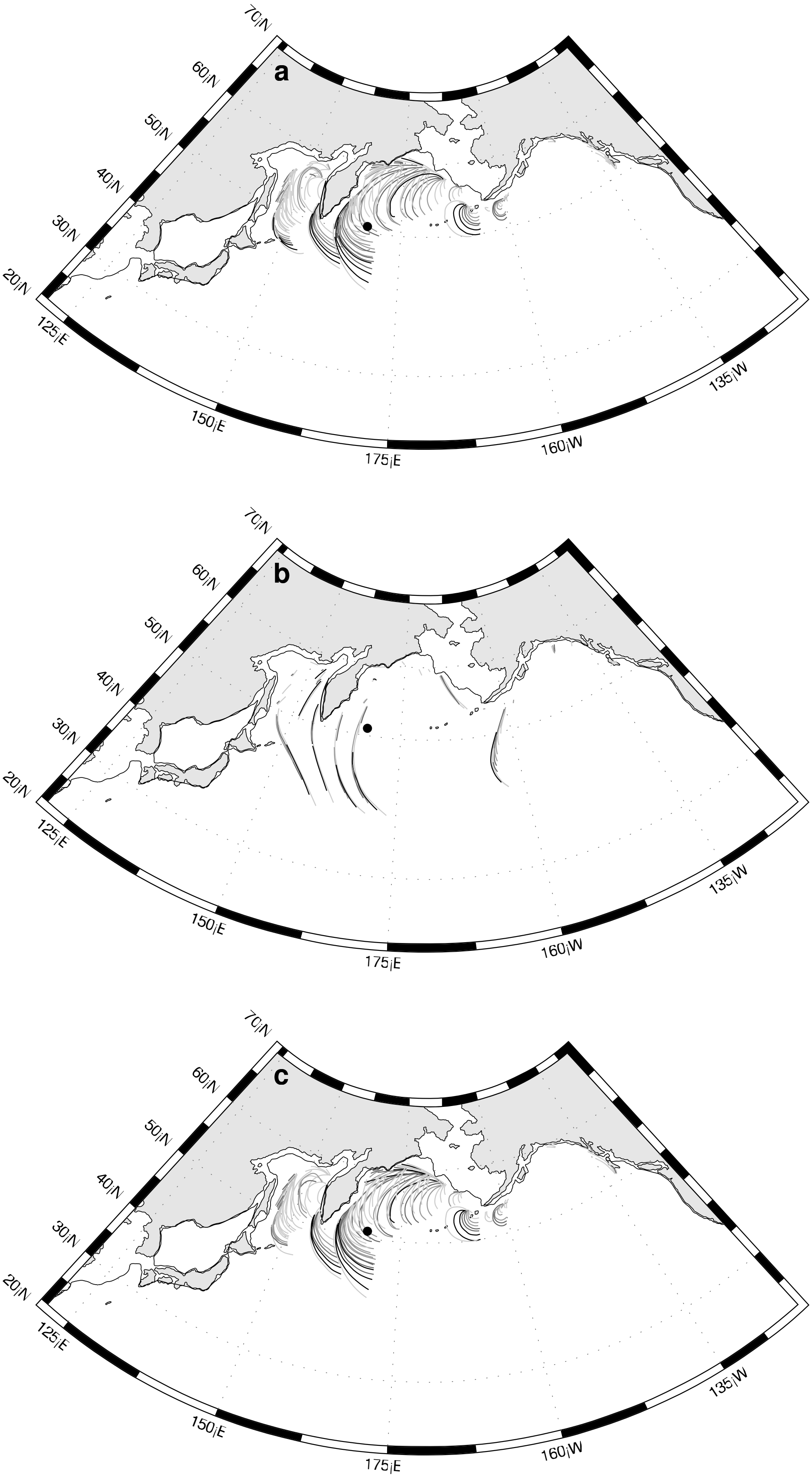

Fig. 3 Modelled iceberg trajectories for the three possible LGM ocean states: a) northern sinking state, b) intermediate sinking state, c) southern sinking state. All three ocean states have similar iceberg trajectories in the Pacific. Note that IRD in the NW Pacific cannot have

been derived from North America. The structure of the trajectories in b) is different due to the different model grid on which the computation was carried out. The location of ODP Site 883 is shown by a black dot.

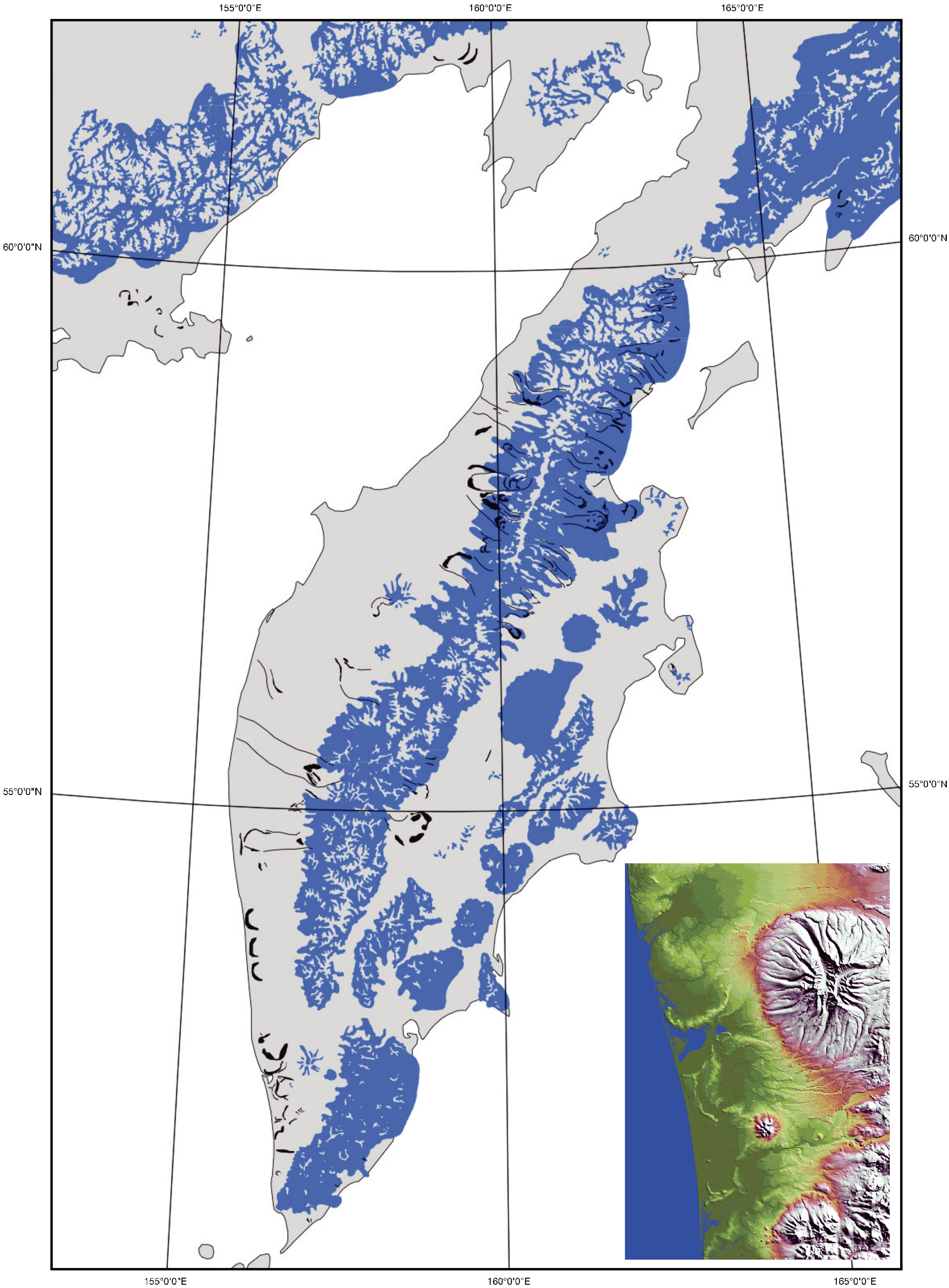

Fig. 4 Kamchatka Peninsula showing the maximal Quaternary glaciation of [28] (blue) and the prominent moraines we identified from imagery (black). Note that some moraine systems

are consistent with the ice extent shown, but that many indicate more extensive ice cover, and reaching the coast. Inset is of the southwest corner of the Peninsula, showing a series of end moraines indicative of ice meeting the coast (see Fig. S4). The dated tephra of [18] were found at three different locations near 53°N 157°E.

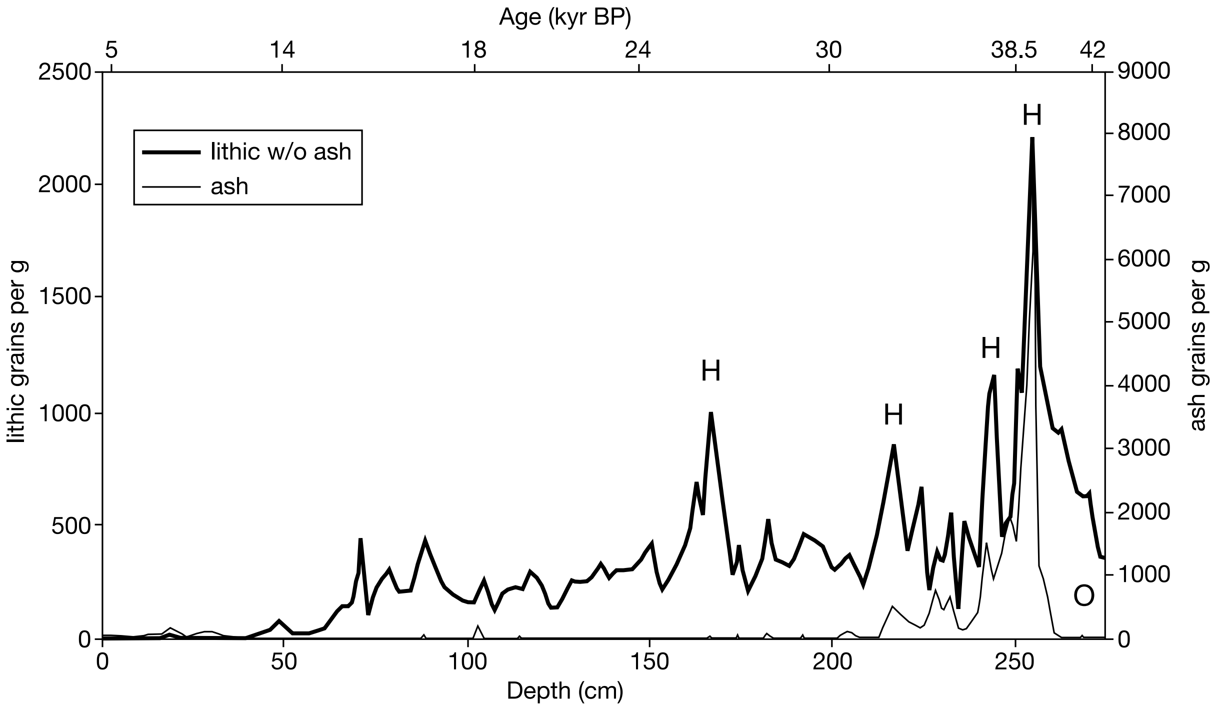

Fig. 5 Variation downcore (883D) of the number of lithic grains per gram, without ash (bold) and ash alone (line). The age model for the core is given along the upper boundary. The ash was counted separately for every other sample so the temporal resolution is reduced compared to the original analysis. The oldest two lithic peaks may be slightly contaminated by material deriving from volcanic eruptions, as there is a particular strong ash signature in the core sediments from 37-39.7 kyr BP, with an extreme peak from a major eruption at 39.3 kyr BP. To quantify this, the typical variation in replicate counts was approximately 10% of the total. The major IRD events are denoted by ‘H’ and the onset of the biggest Heinrich Event, which is dominated by increasing iceberg discharge but no ash deposits, is indicated by ‘O’.

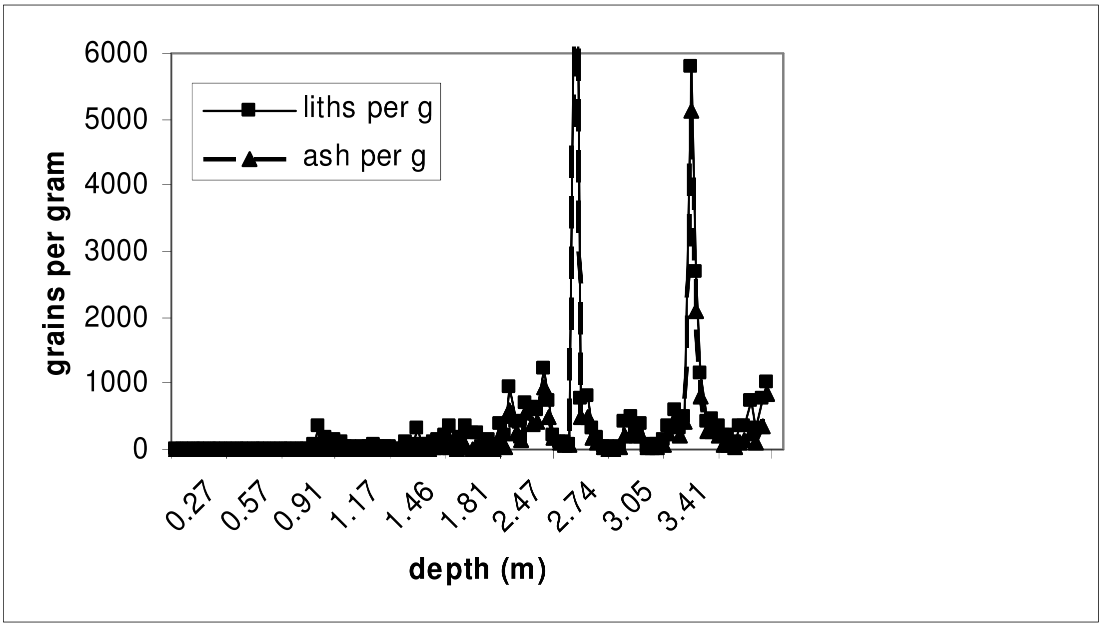

Fig. 6 Variation downcore (883D) of the number of lithic grains per gram, without ash (thin line) and ash alone (bold dashed), from coarser analysis [38] over a longer time period, back to ~ 62 ka BP. The peaks around 2.55 m (~ 41 ka BP) extend to ~ 10,000 grains per gram. Note that the major lithic peaks start rising slightly earlier than the ash peaks in both cases shown.

Table 1

Geochemistry of tephras from the mid-Weichselian (Sartan) region around Kamchatka (%)

Ash	Age (BP)	SiO_2	TiO_3	Al_2O3	FeO	MgO	CaO	K_2O	Na_2O
K2	~25kyr	74	0.3	13	2.3	0.3	1.5	2.5	4
K3	~40-45kyr	74	0.3	13	2.3	0.3	1.5	2.5	4
SW Kam-chatka	>40kyr	73.0	0.3	15.2	2.4	1.2	1.6	2.2	3.9
883B	40kyr	74.1	0.6	15.0	2.3	0.0	1.4	3.8	2.9

K2 and K3 geochemistry averaged from a range of cores in the Sea of Okhotsk and dates [53], SW Kamchatkan date and geochemistry from [18], core 883B geochemistry from Cao et al. (1995) and date from [54].

Supplementary Material

S1. Construction of Figure 2

Table S1 shows the data used in the compilation of Figure 2. There are a variety of different ways in which past research records ice-rafted debris (IRD) measurements. Intrinsically, the most quantitatively unambiguous is the rate measurement in $gcm^{-2}kyr^{-1}$. However, even with this measurement there are various size fractions used. As a basis to separate magnitudes we take the 0.25 $gcm^{-2}kyr^{-1}$ boundary, for the 63-2000 μm size fraction, used by [20], and Hemming (2004), to distinguish between high and low magnitudes of IRD in the glacial central North Atlantic. The two categories **S** and **VS** denote values above this boundary, while F and S denote values below, with X denoting absence of IRD. For a few locations in both the Atlantic and Pacific there exist multiple ways of representing IRD, allowing some degree of comparison between the methods. However, subjective interpretation is sometimes required to produce a final grading. For example, the % dry weight measurement firstly can have various size bands (starting from 63 μm or 500 μm changes the percentage by more than a factor of 10 (Dahlgren and Vorren 2003)), but is also highly dependent on the background marine productivity at the site. Productive sites can have lower IRD percentages, for the same size band, as marine deserts, yet quantitatively the same flux. Similarly, the grains g^{-1} measurement suffers again from the variable size banding (or sometimes none specified), but is also highly dependent on the size of IRD particles. These factors inevitably inflate values for smaller starting fractions, as a lot of small grains can be replaced by few large grains. Thus similar numbers of grains g^{-1} can occur for absolute fluxes differing by a factor of 100 (compare van Kreveld et al. (2000) with [22]). When only core logs are available the grading is even more problematic, and depends on the degree to which sand layers and pebbles occur within the Late Weichselian segment of the core. Thus, while there is an approximate separation of the gradings - ‘F’ denotes concentrations < 50 $mgcm^{-2}kyr^{-1}$, ‘S’ ~ 50-250 $mgcm^{-}$

^{2}kyr^{-1}, ‘**S**’ ~ 250-1000 mgcm^{-2}kyr^{-1} and ‘**VS**’ > 1000 mgcm^{-2}kyr^{-1}, all in the size fraction 63-2000 μm – the reader needs to note the subjective nature of the grading for many sites.

Table S1. Data and references that contributed to LGM maps in Fig. 2. References not in main manuscript are listed below in alphabetically order for each ocean. All data is from the interval 15-21 kyr BP, and much is approximate, representing a background from plots shown in the references.

Pacific				
Location	Reference	Unit	Category	Core/Comment
~ 40°N 135°E	Core logs (Ingle et al. 1975)	No record	X	DSDP Leg 31, Sites 299-302
41.6°N 154.0°E	[21]	~0.01 gcm^{-2}kyr^{-1}	F	DSDP Site 580; 250-2000 μm fraction
38°N 153°E	Krissek et al. (1985)	0%	X	DSDP Site 579; % in 250-2000 μm fraction
56°N 146°W	[23]	1%	F	DSDP Site 178; % in 250 μm-2mm fraction [NB: occasional sandy layer and few pebbles in core log (Musich & Weser 1973)]
47.1°N 161.5°E	Krissek (1995)	0.027 gcm^{-2}kyr^{-1}	S	DSDP Site 881A; 250-2000 μm fraction
51.2°N 167.8°E	Krissek (1995)	0.015 gcm^{-2}kyr^{-1}	S	DSDP Site 883B; > 125 μm fraction
54.4°N 148.5°W	Krissek (1995)	0.042 gcm^{-2}kyr^{-1}	S	DSDP Site 887A; 250-2000 μm fraction
54.4°N 148.5°W	[24]	0.1 gcm^{-2}kyr^{-1}	S	PAR87-10; 180-500 μm fraction
54.4°N 149.5°W	[24]	0.15 gcm^{-2}kyr^{-1}	S	PAR87-01; 180-500 μm fraction
54.4°N 149.5°W	[24]	0.3 gcm^{-2}kyr^{-1}	S	PAR87-02; 180-500 μm fraction
53°N 164.6°E	[27]	10 gcm^{-2}kyr^{-1}	**VS**	RAMA44PC; > 150 μm fraction (~

				1000 grains g^{-1} [36])
50.5°N 167.5°E	[43]	200 grains g^{-1}	S	GC36
49°N 150°E	[43]	7%	**S**	V34-90; > 80 µm % dry weight (cf. 2% in Holocene)
53°N 179°E	[43]	400 grains g^{-1}	**S**	GC11
51.0°N 148.3°E	Gorbarenko et al. (2004)	3500 grains g^{-1}; 5%	**S**	936; > 150 µm % dry weight (sea-ice contamination?)
42°N 161°E	[20]	2.5%	F	V21-148; > 62 µm % dry weight
47°N 180°	[20]	0.05%	X	V20-109; > 62 µm % dry weight
47°N 170°W	[37]	4%	S	RC10-206; > 250 µm % dry weight*
46°N 178°E	[37]	2%	F	RC10-182; > 250 µm % dry weight*
42°N 179°W	[37]	1.9%	F	V20-108; > 250 µm % dry weight*
46°N 160°W	[37]	3%	S	RC11-171; > 250 µm % dry weight*
44°N 162°W	[37]	0.2%	F	V21-173; > 250 µm % dry weight*
48°N 180°	[37]	5%	**S**	V21-172; > 250 µm % dry weight*
50°N 165°W	[37]	5%	**S**	V21-171; > 250 µm % dry weight*
52.6°N 161.2°W	Creager et al. (1973)	Sand layers & scattered pebbles	S	DSDP Site 183; core log
53.7°N 170.9°W	“	Sand layers and a few erratics	F	DSDP Site 184; core log
54.4°N 169.2°W	“	Nothing in right time frame	X	DSDP Site 185; core log
51.1°N 174.0°W	“	Sand layers or odd erratics	F	DSDP Site 186 & 187; core log
53.8°N 178.6°W	“	Nothing	X	DSDP Site 188; core log
54.0°N 170.2°E	“	Nothing	X	DSDP Site 189; core log
55.6°N 171.6°E	“	Sand layers	F	DSDP Site 190; core log
56.9°N 168.2°E	“	Sand layers and odd erratics	F	DSDP Site 191; core log
53.0°N 164.7°E	“	Scattered erratics	S	DSDP Site 192; core log
44.6°N 126.3°W	Musich & Weser (1973)	Nothing	X	DSDP Site 174; core log
44.8°N 125.2°W	“	Nothing	X	DSDP Site 175;

				core log
45.9°N 124.6°W	"	Nothing	X	DSDP Site 176; core log
50.5°N 130.2°W	"	Indistinct sandy layers	F	DSDP Site 177; core log
56.4°N 146.0°W	"	Occasional pebble	F	DSDP Site 179; core log
57.3°N 147.9°W	"	Sand layers and pebbles	S	DSDP Site 180; core log
57.4°N 148.5°W	"	Copious large pebbles	**S**	DSDP Sites 181 & 182; core log
40.8°N 154.5°E	Gardner (1975)	Nothing	X	DSDP Site 303; core log
39.4°N 155.1°E	"	Nothing	X	DSDP Site 304; core log
32.0°N 157.8°E	"	Some pumice & chalk – IRD?	F	DSDP Sites 305 & 306; core log
20-32°N 160°E-170°W	"	Nothing	X	DSDP Sites 307-308, 310-311, 313; core log
42.4°N 170.5°E	Shambach (1980)	Glacial erratics	F	DSDP Site 431; core log
41.3°N 170.4°E	"	Nothing	X	DSDP Site 432; core log
44.8°N 170.0°E	"	Nothing	X	DSDP Site 433; core log
40.6°N 143.3°E	Lee & Stout (1980)	Pebbles	F	DSDP Site 439; core log
39.7°N 143.8°E	"	Evidence of sand layers, pumice and pebbles	F	DSDP Sites 435 & 440-441; core log
31°N 140°E	Barbu & Julson (1990)	Nothing	X	ODP Sites 787-791; core log
32°N 141°E	"	Some pebbles	F	ODP Sites 792-793; core log
48.6°N 123.5°W	Fox (1998a)	Pebbles and sand layers	S	ODP Sites 1033-1034; core log
48.4°N 128.6°W	Fox (1998b)	Nothing	X	ODP Sites 1035-1038; core log
39°N 143.3°E	Lowe (2000)	Some evidence of sand layers	F	ODP Sites 1150-1151; core log
47.9°N 128.6°W	Miller (1998)	Nothing	X	ODP Sites 125-126; core log
41.1°N 160.0°E	Peters (2001)	Nothing	X	ODP Site 1179
Atlantic				
62.7°N 37.5°W	Krissek et al. (2004)	10,000 grains g^{-1}	**VS**	ODP Site 919; > 150 µm fraction
59.2°N 30.9°W	Van Kreveld et	~ 500 grains g^{-1}	S	SO82-05GGC (~

	al. (2000)			10% or 0.08 gcm^{-2}kyr^{-1}, Lackshweitz et al. 1998, > 65 µm % dry weight)
67.1^{o}N 7.1^{o}E	Dahlgren & Vorren (2003)	~0.3 gcm^{-2}kyr^{-1}; ~ 5 gcm^{-2}kyr^{-1}	**VS**	JM98-625/1; 500-2000 µm fraction; 63-2000 µm fraction
40.6^{o}N 9.9^{o}W	de'Abreu et al. (2003)	1-2 %	S	MD95-2040; > 125 µm % dry weight
47^{o}N 8^{o}W	[28]	50 gcm^{-2}kyr^{-1}	**VS**	MD95-2002
49^{o}N 12^{o}W	[28]	10 gcm^{-2}kyr^{-1} ; ~ 400 grains g^{-1}	**VS**	NKS512; > 150 µm fraction
48.4^{o}N 25.1^{o}W	[28]	3 gcm^{-2}kyr^{-1}	**VS**	T88-9P; > 65 µm fraction
62.7^{o}N 4.0^{o}W	[28]	19 gcm^{-2}kyr^{-1}	**VS**	ENAM93-21
48.8^{o}N 12.6^{o}W	[28]	15 gcm^{-2}kyr^{-1}	**VS**	OM-5-K
41.5^{o}N 9.7^{o}W	[28]	17 gcm^{-2}kyr^{-1}	**VS**	PO28-1
49.9^{o}N 24.2^{o}W	Bond et al. (1992)	~ 10 gcm^{-2}kyr^{-1}; 15-20% (Hemming, 2004)	**VS**	ODP Site 609; > 150 µm % dry weight
54.9^{o}N 16.6^{o}W	Richter et al. (2001)	~ 2000 grains g^{-1}; 10%	**VS**	ENAM97-09; > 150 µm fraction, % dry weight
64.9^{o}N 29.3^{o}W	Hagen & Hald (2002)	~ 20 grains g^{-1}	S	JM96-1225; > 500 µm fraction
60.3^{o}N 9.8^{o}W	[44]	~ 2000 grains g^{-1}	**VS**	ENAM32; > 125 µm fraction
63^{o}N 59^{o}W	Andrews & Barber (2002)	2-4%	S	HU87-009; 65-2000 µm % dry weight
59.4^{o}N 31.1^{o}W	Lackschewitz et al. (1998)	~ 20%	**S**	SO82-2; > 63 µm % dry weight
59.0^{o}N 31.1^{o}W	"	~ 25%	**S**	LO09-23
54^{o}N 17^{o}W	"	300 grains g^{-1}	S	VM23-81
67^{o}N 3^{o}W	"	60%; 0.5-1 gcm^{-2}kyr^{-1}	**S**	23071; > 63 µm % dry weight
42^{o}N 55^{o}W	Hemming (2004)	20%	**S**	CH69-K09; > 150 µm % dry weight
43^{o}N 51^{o}W	"	>40%	**VS**	V23-14; > 150 µm % dry weight
43^{o}N 30^{o}W	"	20%	**VS**	SU90-08; > 150 µm % dry weight
49^{o}N 23^{o}W	"	20%; 2000 grains g^{-1}	**VS**	V28-82; ; > 150 µm % dry weight
47^{o}N 20^{o}W	"	15%	**S**	ME69-17; 180-3000 µm % dry weight

* dating not certain – not used in Fig. 2 but supporting pattern.

Pacific

E.M. Barbu, A.P. Julson (eds.) Init. Rep. ODP 126 (1990) doi:10.2973/odp.proc.ir.126.1990.

J.S. Creager, D.W. Scholl, P.R. Supko (eds.) Init. Rep. DSDP 19 (1973) doi:10.2973/dsdp.proc.19.1973.

G.L. Fox (ed.) Init. Rep. 169S (1998a) doi:10.2973/odp.proc.ir.169s.1998.

G.L. Fox (ed.) Init. Rep. 169 (1998b) doi:10.2973/odp.proc.ir.169.1998.

J.V. Gardner (ed.) Init. Rep. DSDP 32 (1975) doi:10.2973/dsdp.proc.32.1975.

S.A. Gorbarenko, J.R. Southon, L.D. Keigwin, M.V. Cherepanova, I.G. Gvodzeva. Late Pleistocene-Holocene oceanographic variability in the Okhotsk Sea: geochemical, lithological and paleontological evidence. Palaeogeog. Palaeoclimatol. Palaeoecol. 209 (2004) 281-301.

J.C. Ingle Jr., D.E. Karig, S.M. White. (eds.) Init. Rep. DSDP 31 (1975) doi:10.2973/dsdp.proc.31.1975

L.A. Krissek, J.J. Morley, D.K. Lofland. The occurrence, abundance, and composition of ice-rafted debris in sediments from Deep Sea Drilling Project Sites 579 and 580, northwest Pacific. In G.R. Heath, L.H. Burkle, et al. (eds.) Init. Rep. DSDP 86 (1985) Washington (U.S. Government Printing Press), 647-655.

L.A. Krissek. Late Cenozoic ice-rafting records from Leg 145 sites in the North Pacific: Late Miocene onset, Late Pliocene intensification, and Pliocene-Pleistocene events. In D.K. Rea, I.A. Basov, D.W. Scholl, J.F. Allan (eds.) Proc. Ocean Drill. Prog. Sci. Res. 145 (1995) 179-194.

M. Lee, L.N. Stout (eds.) Init. Rep. DSDP 56/57 (1980) doi:10.2973/dsdp.proc.5657.1980.

G. Lowe (ed.) Init. Rep. 186 (2000) doi:10.2973/odp.proc.ir.186.2000.

A.T. Miller (ed.) Init. Rep. 168 (1998) doi:10.2973/odp.proc.ir.168.1998.

L.F. Musich, O.E. Weser (eds.) Init. Rep. DSDP 18 (1973) doi:10.2973/dsdp.proc.18.1973.

L.L. Peters (ed.) Init. Rep. 191 (2001) doi:10.2973/odp.proc.ir.191.2001.

J. Shambach (ed.) Init. Rep. DSDP 55 (1980) doi:10.2973dsdp.proc.55.1980.

Atlantic

J.T. Andrews, D.C. Barber, Dansgaard-Oeschger events: is there a signal of the Hudson Strait ice stream? Quater. Sci. Rev. 21 (2002) 443-454.

G. Bond, H. Heinrich, W. Broecker, L. Labeyrie, J. McManus, J. Andrews, S. Huon, R. Jantschik, S. Clasen, C. Simet, K. Tedesco, M. Klas, G. Bonani, S. Ivy, Evidence for massive discharges of icebergs into the North Atlantic ocean during the last glacial period, Nature 360 (1992) 245-249.

K.I.T. Dahlgren, T.O. Vorren, Sedimentary environment and glacial history of the last 40 ka of the Vørren continental margin, central Norway, Mar. Geol. 193 (2003) 93-127.

L. De'Abreu, N.J. Shackleton, J. Schönfeld, M. Hall, M. Chapman, Millennial-scale oceanic climate variability off the western Iberian margin during the last two glacial periods, Mar. Geol. 196 (2003) 1-20.

S. Hagen, M. Hald, Variation in surface and deep water circulation in the Denmark Strait, North Atlantic, during marine isotope stages 3 and 2, Paleoceanogr. 17 (2002) doi:10.1029/2001PA000632.

S.R. Hemming, Heinrich events: massive Late Pleistocene detritus layers of the North Atlantic and their global climate imprint, Rev. Geophys. 42 (2004) doi:10.1029/2003RG000128.

S. van Kreveld, M. Sarnthein, H. Erlenkeuser, P. Grootes, S. Jung, M. J. Nadeau, U. Pflaumann, A. Voelker, Potential links between surging ice sheets, circulation changes, and the Dansgaard-Oeschger cycles in the Irminger Sea, 60 - 18 kyr, Paleoceanogr. 15 (2000) 425-442.

K.S. Lackschewitz, K.-H. Baumann, B. Gehrke, H.-J. Wallrabe-Adams, J. Thiede, G. Bonani, R. Endler, H. Erlenkeuser, J. Heinemeier, North Atlantic ice sheet fluctuations 10,000-70,000 years ago as inferred from deposits on the Reykjanes Ridge, southeast of Iceland, Quater. Res. 49 (1998) 171-182.

T.O. Richter, S. Lassen, Tj.C.E. van Weering, H. de Haas, Magnetic susceptibility patterns and provenance of ice-rafted material at Feni Drift, Rockall Trough: implications for the history of the British-Irish ice sheet, Mar. Geol. 173 (2001) 37-54.

S2. Remote Sensing Images

The following figures illustrate and report some of the glacial geomorphological evidence discovered and that have been used to demarcate the extent of palaeo ice masses. Our conclusion about a two-stage glaciation style (Figs. 1 and 4 of main text) is based on such evidence. 105 moraines have been identified, some of which are shown here.

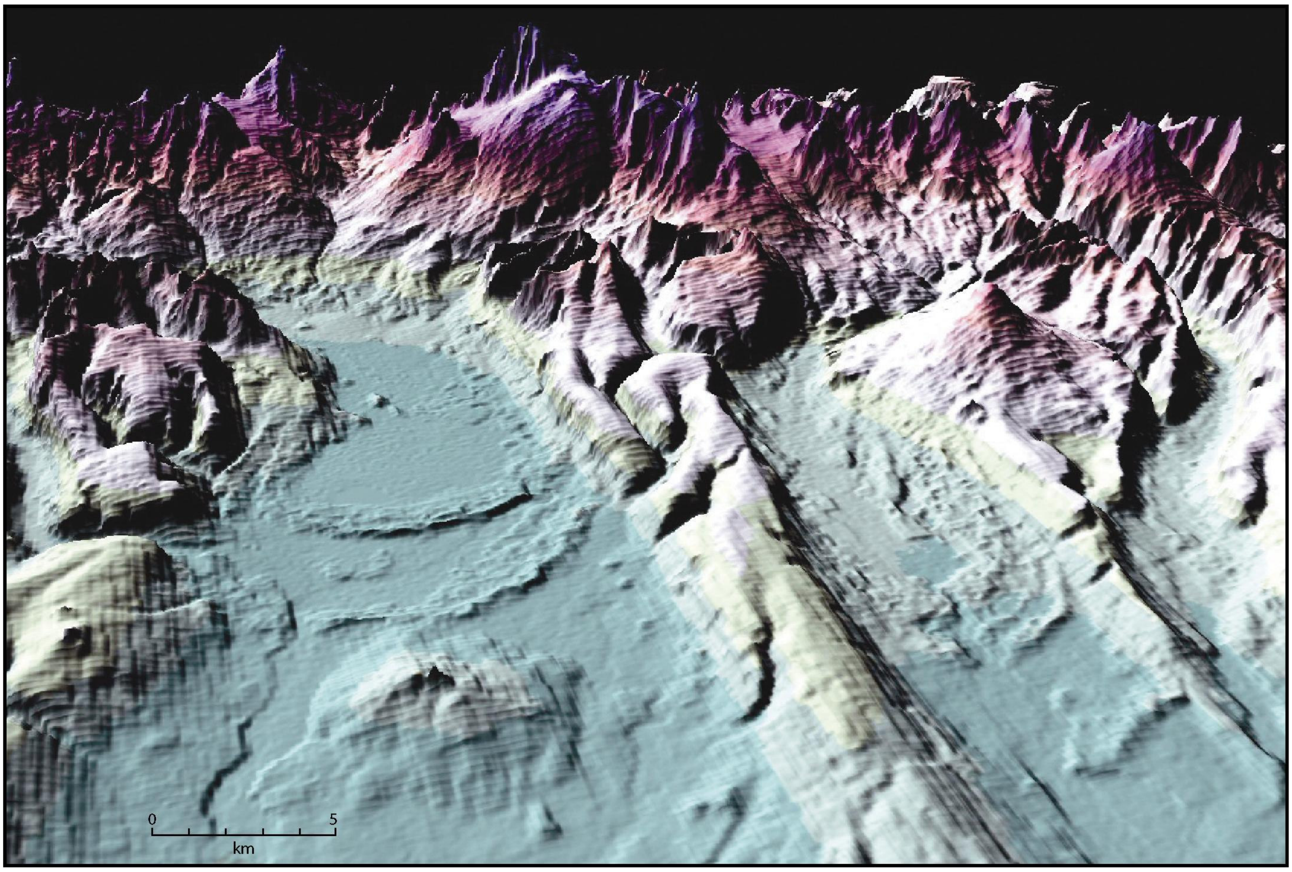

Figure S1. This shows a sequence of end and lateral moraines recording glacier retreat in these two valleys on the western flank of the main median (Sredinny) ridge of Kamchatka. Image is a 3-D visualisation (looking east) of Shuttle Radar Topography Mission (SRTM) elevation data and is centred at 160^0 8’ E; 57^0 58’ N, with a foreground width of ca. 35 km.

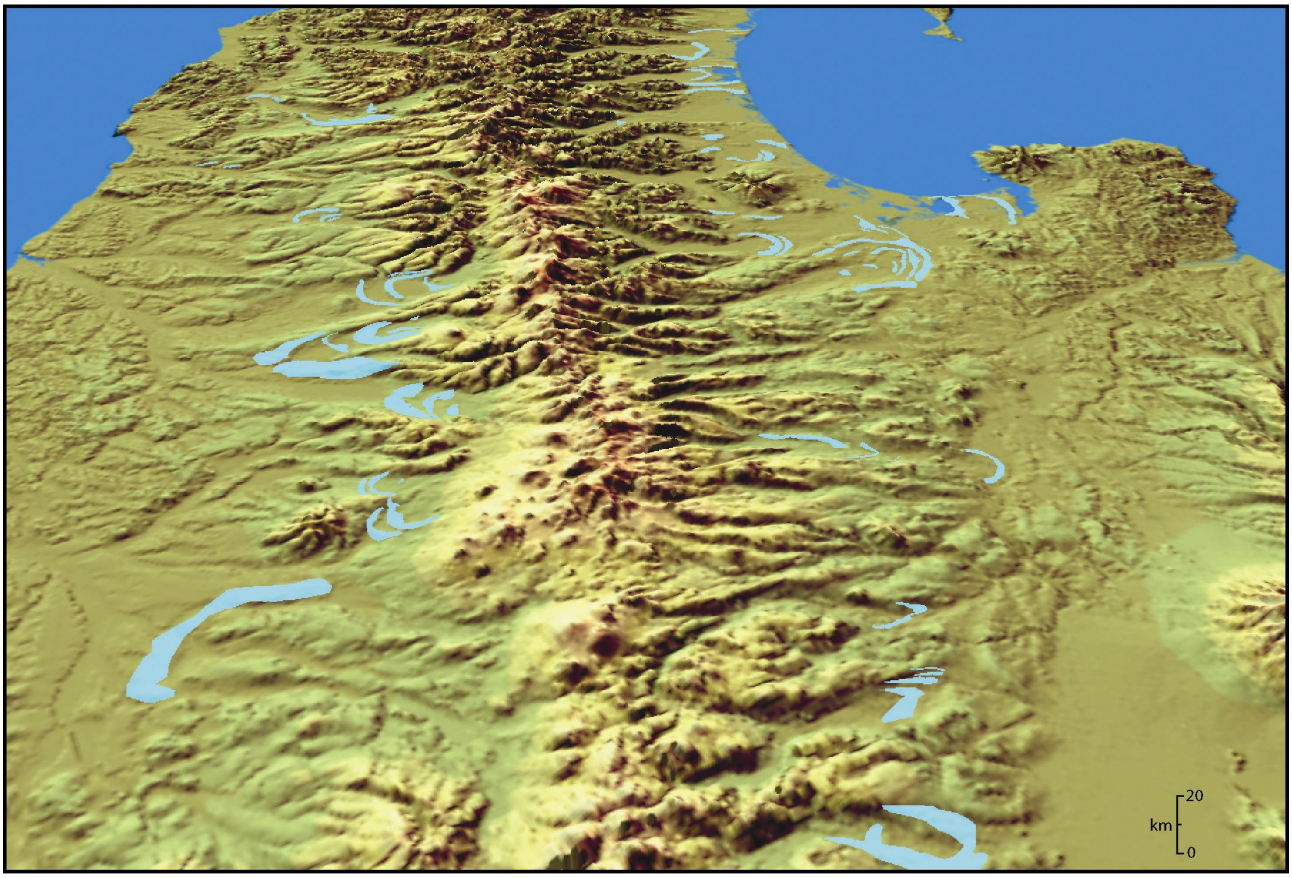

Figure S2. Moraine distribution on the west and east flanks of the main median ridge of Kamchatka. Note that end moraines occupy all major valleys and are positioned approximately symmetrically around the main divide. We take this systematic pattern to indicate approximately synchronous end moraine formation recording a stable margin configuration of a major icefield centred over the high ground. These moraines are consistent with previously reconstructed LGM ice extent [35], which is portrayed in Figs. 1 and 4 of the main text. Image is a 3-D visualisation of SRTM elevation data, looking NNE from ca. 159^0 21' E; 56^0 32' N, for a distance of around 300 km.

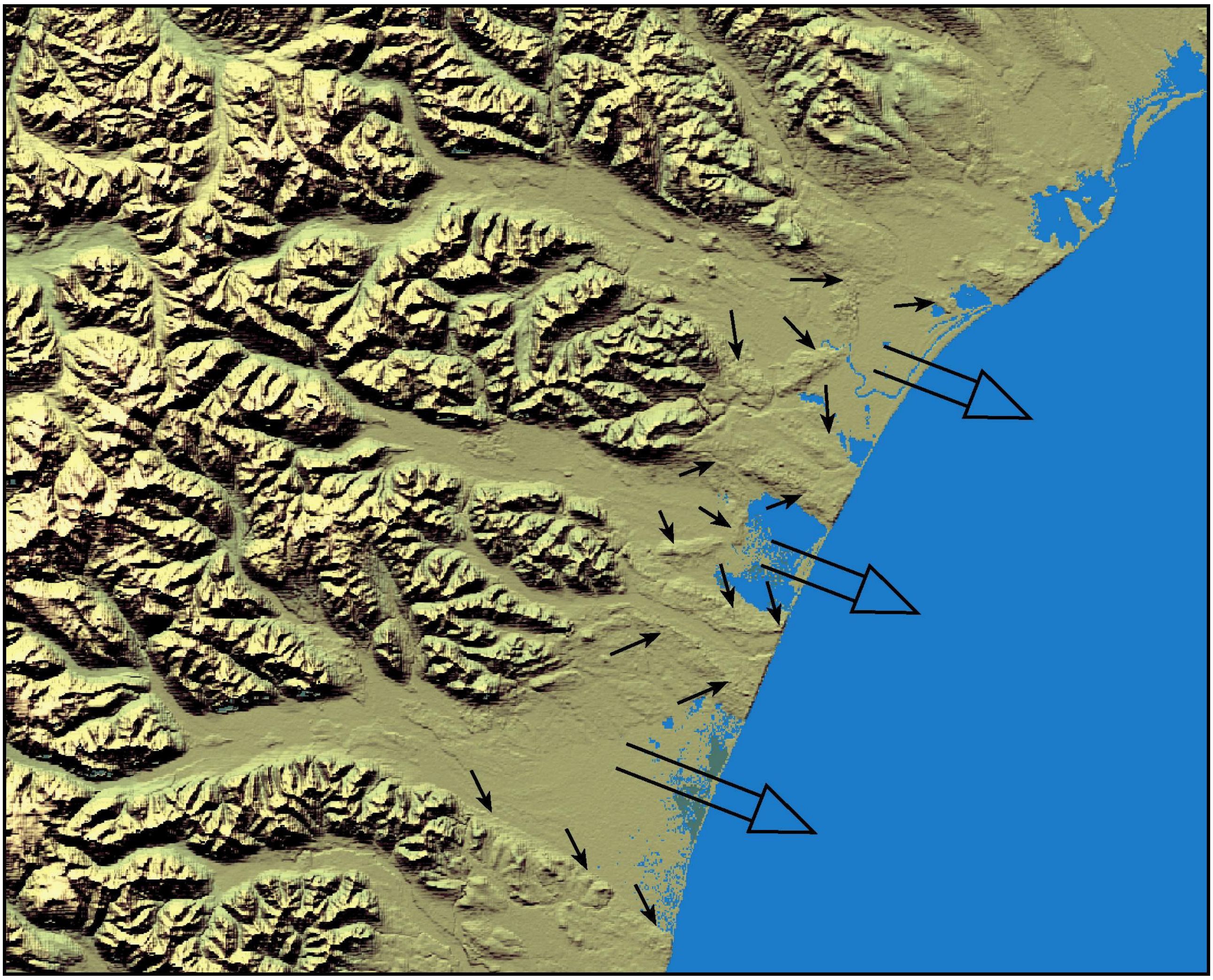

Figure S3. On parts of the eastern shore of Kamchatka, glacier trimlines and moraines indicate that ice outlets drained directly into the sea. Here lateral moraines are evident extending to the present day shoreline and end moraines are visible which we interpret as indicating a stillstand of the margin once ice retreated back onto land. This is consistent with the LGM ice extent previously reconstructed [35]. Visualisation of SRTM elevation data, centred on 161^0 50’ E; 58^0 41’ N, and image is 100 km across.

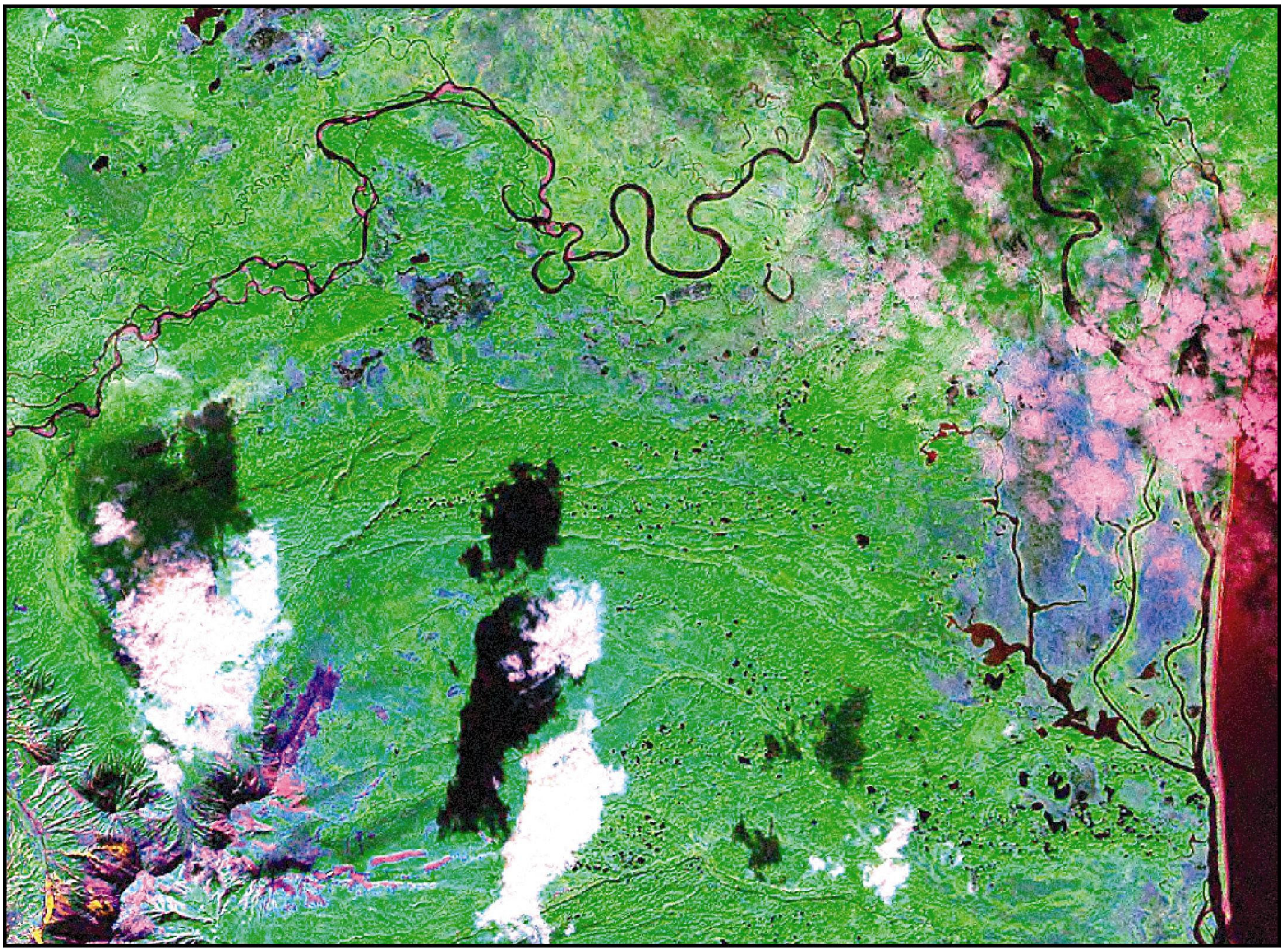

Figure S4. In the centre of this satellite image (Landsat ETM+), to the west and east of the prominent cloud shadow, are a series of channels mostly aligned west-east and which closely parallel contours along the valley flank. The topographic context of the channels is such that they cannot have been cut by present day water drainage. We interpret these as lateral channels eroded by meltwater flowing along a glacier margin. They are at 170 m above sea level and only 8 km from the present-day shoreline. A lateral margin of an outlet glacier positioned to create such channels must have extended offshore. Image is 20 km across and is centred on 161^{0} 49’ E; 58^{0} 07 N. The coastline is visible in the southeast of the image.

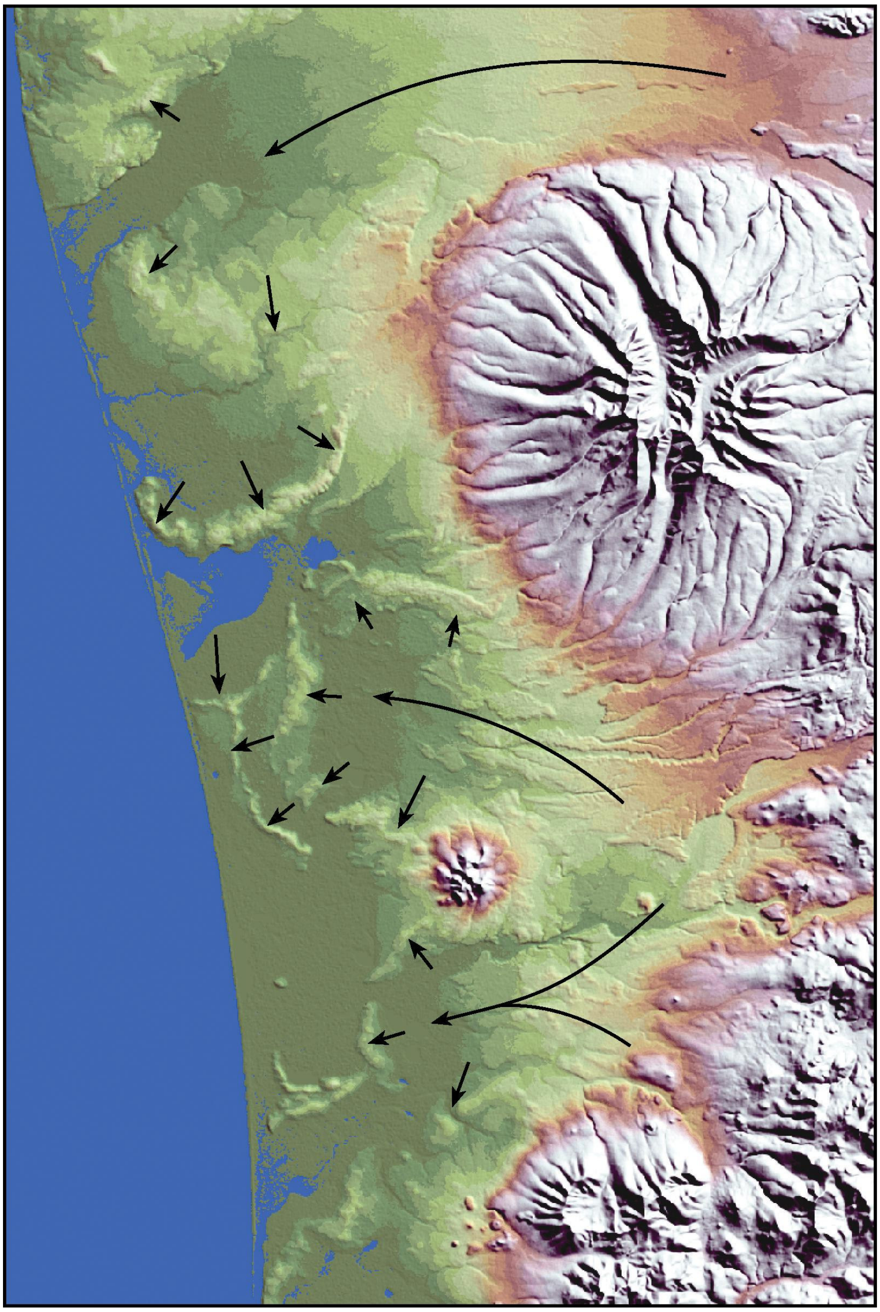

Figure S5. On the west coast of Kamchatka numerous moraine systems are evident close to the present day coastline. This visualisation of SRTM elevation data clearly depicts end moraines at or near the coast and we infer that a major stillstand of the ice margin occurred in order to generate them. Note that the two main volcanoes acted as obstacles (likely as nunataks), diverting ice flow around them, and in the case of the large volcano, such that two ice lobes nearly coalesced in its lee. Ice extent along this west coast, as recorded by moraines is not consistent with previously mapped extents [35]. In his reconstruction both the LGM and Quaternary maximum extent of ice cover is restricted to an ice field along the main median ridge, with ice nowhere reaching the western coastline (and see Fig. 4, in main text). Our mapping demonstrates that ice definitely reached the coast, and we presume, likely beyond it with the margin stabilising once it retreated onto land. Image is centred on 156^{0} 43 E; 52^{0} 28 N, and is 75 km across.

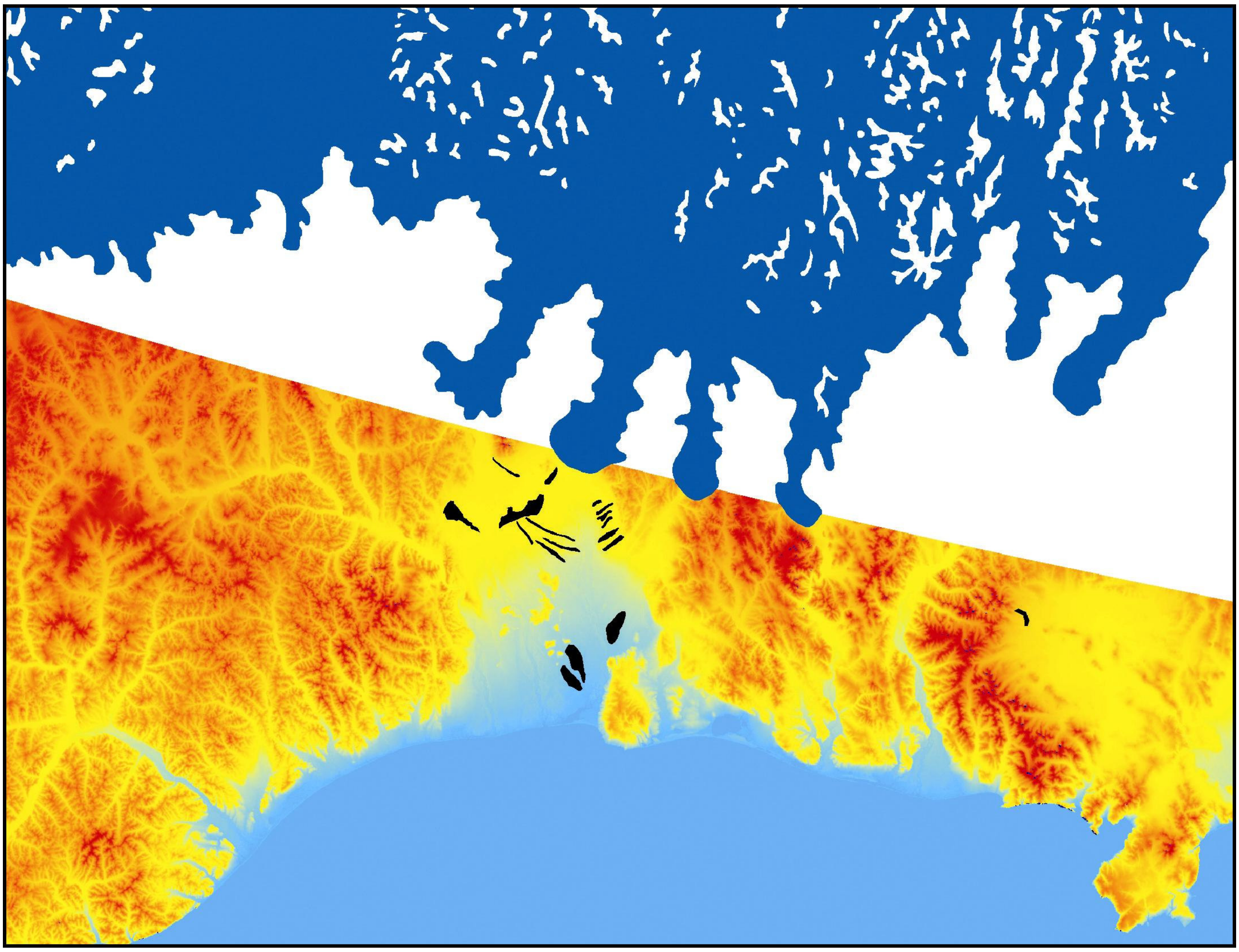

Figure S6. On the northern shore of the Sea of Okhotsk, near the city of Okhotsk, a similar pattern emerges; end moraines are found near the coast and some 60 km further out than the LGM extent previously mapped [35]. Moraines in black are shown on top of a coloured rendition of elevation. Zamoruyev's [35] LGM extent is marked in blue. Elevation data is from SRTM whose northern limit of this dataset is clear to see. Image is centred on 143^{0} 13' E; 59^{0} 50' N, and is 350 km in width.